Hydrogen Sensing with Diameter- and Chirality-Sorted Carbon Nanotubes

Marc Ganzhorn,[†,‡,△,*] Aravind Vijayaraghavan,[†,▼] Simone Dehm,[†] Frank Hennrich,[†] Alexander A. Green,[§] Maximilian Fichtner,[†] Achim Voigt,[⊥] Michael Rapp,[⊥] Hilbert von Löhneysen,[‡,∥,#] Mark C. Hersam,[§] Manfred M. Kappes,[¶,#] and Ralph Krupke[†,#,*]

[†]Institut für Nanotechnologie, Karlsruhe Institute of Technology, 76021 Karlsruhe, Germany, [‡]Physikalisches Institut, Karlsruhe Institute of Technology, 76128 Karlsruhe, Germany, [▼]School of Computer Science, The University of Manchester, Manchester M13 9PL, U.K., [§]Department of Materials Science and Engineering and Department of Chemistry, Northwestern University, Evanston, Illinois 60208-3108, United States, [⊥]Institut für Mikrostrukturtechnik, Karlsruhe Institute of Technology, 76021 Karlsruhe, Germany, [∥]Institut für Festkörperphysik, Karlsruhe Institute of Technology, 76021 Karlsruhe, Germany, [¶]Institut für Physikalische Chemie, Karlsruhe Institute of Technology, 76128 Karlsruhe, Germany, [#]DFG Center for Functional Nanostructures (CFN), 76028 Karlsruhe, Germany. [△]Present address: Institut Néel, CNRS-UJF Grenoble, BP 166, 38042 Grenoble, France.

ABSTRACT The work function of palladium is known to be sensitive to hydrogen by the formation of a surface dipole layer or Pd hydride. One approach to detect such a change in the work function can be based on the formation of a Schottky barrier between the palladium metal and a semiconductor. Here, we study the hydrogen sensitivity of Schottky barrier field-effect transistors made for the first time from diameter- and chirality-sorted semiconducting single-walled carbon nanotubes (s-SWNTs) in contact with Pd electrodes. We observe an unrivaled 100-fold change in the on-state conductance at 100 ppm H_2 compared to air for devices with s-SWNT and diameters between 1 and 1.6 nm. Hydrogen sensing is not observed for devices of Pd-contacted few-layer graphene (FLG), as expected due to the absence of a significant Schottky barrier. Unexpectedly, we observe also a vanishing sensitivity for small-diameter SWNTs. We explain this observation by changes in the nanotube work function caused by spillover and chemisorption of atomic hydrogen onto small-diameter nanotubes. We also observe that long-term sensing stability is only achieved if the gate voltage is inverted periodically. Under constant gate bias, the sensitivity reduces with time, which we relate to gate screening by accumulated charges in the substrate.

KEYWORDS: single-walled carbon nanotube · chirality · diameter · hydrogen · sensing · sorting · Schottky barrier field-effect transistor

The use of hydrogen as an energy carrier in hydrogen-based storage and transfer would generate a considerable demand of hydrogen sensors that are sensitive, reliable, cost-effective, and small.[1,2] Today, commercial sensors are based on electrochemical response,[3] mass spectrometry,[4] measurement of electrical resistance,[5] and measurement of thermal conductivity.[6,7] For mass applications, sensors based on resistance changes are most attractive because they are easy to miniaturize and to integrate into read-out electronics. Their central sensing unit can be either a field-effect transistor with a hydrogen-sensitive (catalytic) gate electrode[8] or a hydrogen-sensitive material.[5] A prominent and well-studied example for a hydrogen-sensitive material is palladium, which changes its volume and resistance under hydrogen loading.[5] Recently, this system has gained a lot of attention by the use of Pd nanoparticles with a large surface-to-volume ratio, which yielded very short response time.[5,9,10] At low hydrogen partial pressure, these changes are small, imposing a fundamental limitation of this sensing principle, besides stress-induced failure upon repeated cycling. An alternative to the measurements of bulk property would be a surface-sensitive technique that is able to detect changes of the Pd surface caused by atomic hydrogen H. For instance, a dipole layer of H is formed at low H_2 partial pressure by the dissociation of the molecular hydrogen, leading to an increase of the work function of Pd.[11] At higher H_2 partial pressure, hydrogen diffuses into the Pd bulk, forming Pd hydride and hence reducing the Pd work function.[12] A Schottky barrier, which forms at the interface between a metal and a semiconductor, could be a useful sensing element because the electric current through a Schottky barrier depends exponentially on the work functions of the two materials.[13] For macroscopic Schottky barriers, however, hydrogen would have to diffuse through either the Pd or the semiconductor to reach the barrier, likely with detrimental effects on the response dynamics. A nanoscale Schottky barrier contact, instead, is "open" to the gas atmosphere because of its contact geometry and would allow unhindered hydrogen diffusion to the barrier.

Nanoscale transistors based on semiconducting single-walled carbon nanotubes

*Address correspondence to marc.ganzhorn@grenoble.cnrs.fr, ralph.krupke@kit.edu.

Received for review August 11, 2010 and accepted February 10, 2011.

Published online February 22, 2011
10.1021/nn101992g

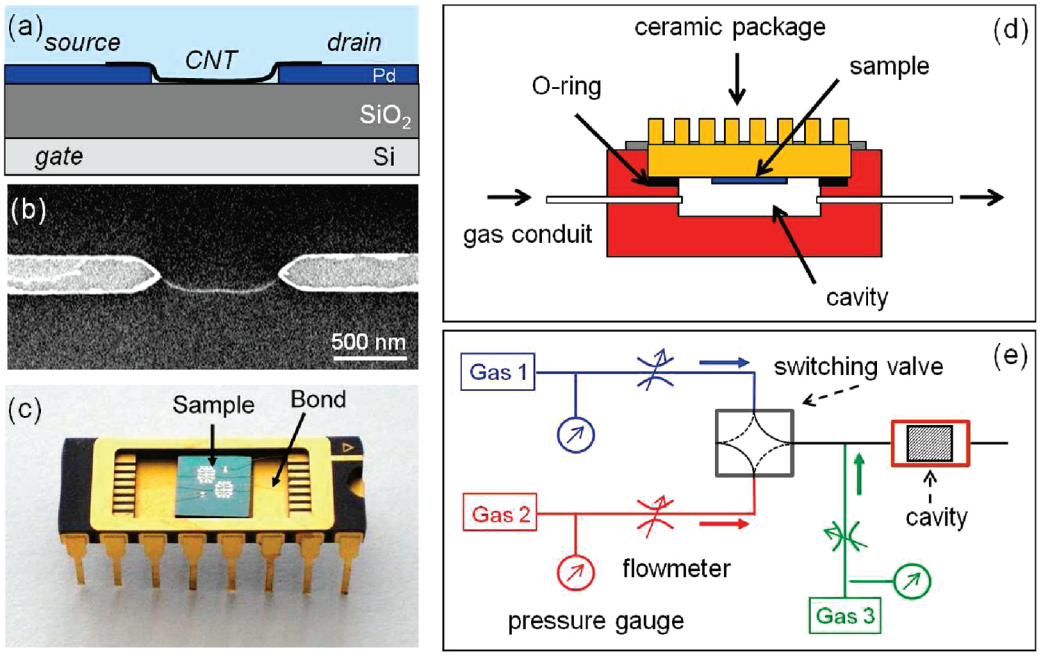

Figure 1. (a) Cross-sectional schematic of a CNT-FET device. (b) Voltage−contrast scanning electron micrograph of a 1.4 nm s-SWNT/Pd FET (750 nm device channel length). (c) Devices are bonded into a ceramic package and (d) mounted upside down onto an open gas cavity. (e) Cavity is connected to a gas line system, allowing switching between gas flow 1 and 2 and optional mixing with gas flow 3.

(s-SWNTs) are known to operate as Schottky barrier field-effect transistors (SB-FETs), with the transconductance limited by the transmission of the barrier and not by the conductance of the channel.[14] SB-FETs formed by s-SWNTs and Pd source and drain electrodes are also sensitive to hydrogen, as expected.[15] However, the hydrogen sensitivity of pristine nanotube-based SB-FET[15−19] and Pd-coated nanotube devices has been rather low,[20−26] most likely due to the use of unsorted carbon nanotube material with non-uniform electronic properties, such as mixed metallic and s-SWNTs with different diameters or multiwalled carbon nanotubes. Here we use selected s-SWNTs with defined structural and electronic properties, given by their diameter d and chiral indices (n,m), for the fabrication of SB-FET hydrogen sensors. We provide data on the sensitivity, the response time, and the long-term stability of s-SWNT-based sensors with chirality-sorted (9,7), (7,6), and (6,5) s-SWNTs and diameter-sorted s-SWNTs with $d = 1.4 \pm 0.2$ nm and describe how the sensor lifetime depends on the measurement protocol.

RESULTS AND DISCUSSION

All devices show enhanced p-type conductance under negative gate bias, typical for s-SWNTs in contact with Pd (Figure S5 in Supporting Information). The on-state conductance, $G_{ON} = I_{SD,ON}/V_{SD,ON}$, is reached for all devices around $V_G = -20$ V, with a weak dependence on V_{SD}. G_{ON} is reduced under hydrogen exposure. Surprisingly, the sensitivity depends strongly on the chirality and diameter of the nanotube. Figure 2 compares the time-dependent response of G_{ON} of 1.4 nm s-SWNT/Pd, (9,7)-SWNT/Pd, (7,6)-SWNT/Pd, and (6,5)-SWNT/Pd FETs under switching between air and H_2/Ar. G_{ON} has been measured at $V_G = -20$ V and $V_{SD} = 0.5$ V under alternating gate-bias operation for reasons explained below. The response to 100 ppm H_2 in Ar for 1.4 nm s-SWNT devices is characterized by a change of the G_{ON} by 3 orders of magnitude at a rate of one decade per 16 s. An overall similar response is observed for the (9,7) devices with, however, two characteristic time scales: an initial fast response, where G_{ON} changes with a rate of one decade per 30 s; and a slow response, where the steady state is reached on the time scale of hours. The change of G_{ON} within the fast response is on the order of one and two decades for the switching air → H_2/air and H_2/air → air, respectively. In the steady state, G_{ON} for 100 ppm H_2 in Ar is suppressed by a factor 500 compared to G_{ON} in air. For (7,6) devices, the response is much lower and weaker, with an extrapolated rate of one current decade per ~8 min. No time dependence was found for the (6,5) devices prepared from both POL#4 and DGU#2 dispersions. We observe a similar behavior with devices prepared on parylene-C-coated substrates, however, with a reduced overall sensitivity (Figure 3 and Figure S6 in Supporting Information). Annealing such devices in air at 200 °C improves their sensitivity as shown in Figure 5.

The sensitivity of s-SWNT-based SB-FET to hydrogen has been reported before in ref 15 and was assigned to changes in the work function of Pd, Φ_{Pd}. Here we observe that the sensitivity of our devices depends on

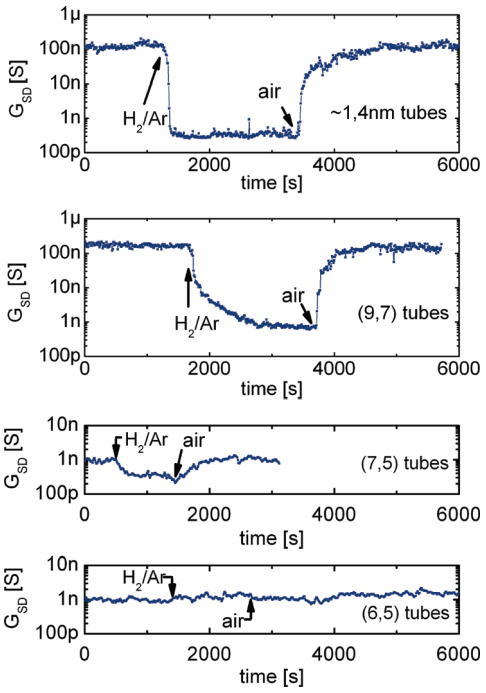

Figure 2. On-state source−drain conductance $G_{ON} = I_{SD}/V_{SD}$ *vs* time, recorded at $V_G = -20$ V and $V_{SD} = 0.5$ V under alternating gate-bias operation. The as-prepared devices were subsequently exposed to air, 100 ppm H_2 in Ar, and air. Traces recorded with 1.4 nm s-SWNT/Pd, (9,7)-SWNT/Pd, (7,6)-SWNT/Pd, and (6,5)-SWNT/Pd FETs on Si/SiO_2 are shown from top to bottom.

the type of s-SWNT, which is difficult to understand solely on changes of Φ_{Pd}, and requires considering the interaction of hydrogen with SWNTs. Since the chiral angles θ of the (9,7), (7,6), and (6,5) SWNTs are very close, with $\theta = 25.9-27.5°$, we assume that the type dependence is in fact a dependence on the nanotube diameter d.

Indeed, if we plot the ratio of the on-state conductance measured in air and in H_2, $G_{ON}^{air}/G_{ON}^{H_2}$ *versus* d, we see that the sensitivity to H_2 is very small for $d = 0.75$ nm and then increases strongly (Figure 3). The maximum sensitivity, that is, current suppression for hole carriers, is found in SB-FETs with a SWNT diameter of $1.1 \text{ nm} < d < 1.4 \pm 0.2$ nm. This can be explained by a decrease of Φ_{Pd}, caused by dissolution of hydrogen into the Pd and a hydrogen surface dipole layer.[12] However, an explanation for the reduced or diminished response of (7,6) and (6,5) devices is required because the Pd electrodes are identical for all SB-FETs. From the gate dependence of I_{SD}, we derive that Schottky barriers form the prime bottleneck for carrier transport in all devices, and hydrogen-insensitive contact resistances can be neglected (Figure S5 and Figure 5).

We propose a model in which we consider changes of the nanotube work function Φ_{CNT} due to hydrogen adsorbed at the SWNT. The model is based on measurements and calculations on the physisorption and chemisorption of molecular and atomic hydrogen,

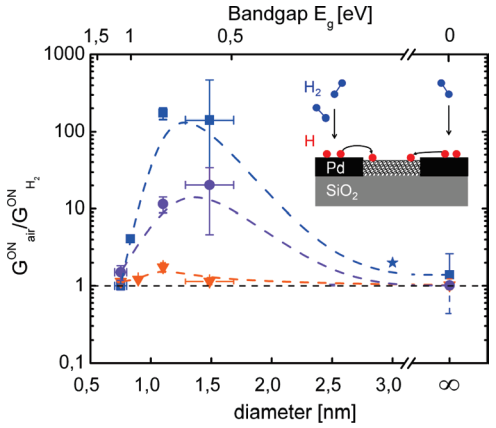

Figure 3. Sensitivity $G_{ON}^{air}/G_{ON}^{H_2}$ of FET devices *vs* SWNT diameter d and electronic band gap $E_g = 2a_{c-c}\gamma_0/d$, with $\gamma_0 = 2.9$ eV and $a_{c-c} = 0.14$ nm.[47] The on-state conductance in air and in 100 ppm H_2 in Ar, G_{ON}^{air} and $G_{ON}^{H_2}$, has been measured under equilibrium conditions. Data are shown for FETs based on s-SWNTs with $d = 1.4 \pm 0.2$ nm, (9,7) tubes with $d = 1.1$ nm, (7,6) tubes with $d = 0.89$ nm, (7,5) tubes with $d = 0.83$ nm, (6,5) tubes with $d = 0.75$ nm, and zero-curvature sp^2 carbon (FLG), indicated by $d \rightarrow \infty$. Three types of s-SWNT FETs have been investigated: s-SWNT/Pd FETs on Si/SiO_2 (blue squares), s-SWNT/Au FETs on Si/SiO_2 (red triangles), and s-SWNT/Pd FETs on Parylene-C coated Si/SiO_2 (purple circles). Data of an s-SWNT/Pd FET with $d = 3$ nm from ref 15 (0.5% H_2) is labeled with a blue star. The dashed lines are guides to the eye, indicating an optimum sensitivity at $d \approx 1-1.5$ nm and vanishing sensitivity for large and small SWNT diameters. The inset illustrates the formation of atomic hydrogen on the Pd surface and its diffusion to and chemisorption on small-diameter s-SWNTs in a device configuration.

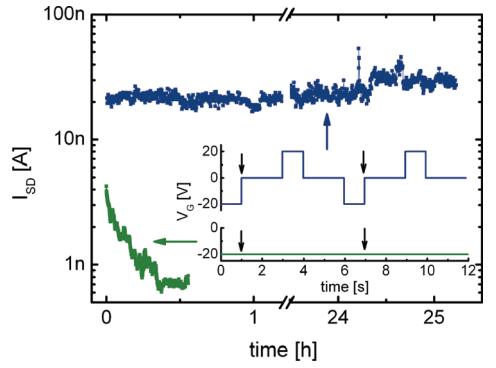

Figure 4. Stability of the source−drain current I_{SD} of a s-SWNT/Pd FET on Si/SiO_2 measured at $V_{SD} = 0.5$ V. The two traces show measurements obtained with different gate-voltage protocols (inset). I_{SD} decreases under constant V_G (green) but remains constant under alternating V_G (blue). The arrows indicate the point in time of recording I_{SD}. I_{SD} has been measured at $V_G = -20$ V for both gate-voltage protocols.

respectively, on sp^2-hybridized carbon surfaces.[27] It has been shown that physisorption on such surfaces is very weak for ambient temperatures. Chemisorption of atomic hydrogen H, however, can be significant for curved sp^2-hybridized carbons, which is the case for C_{60} ($d = 0.71$ nm).[28] On flat graphite surfaces, chemisorption of thermalized hydrogen does not occur.[29] The dependence of chemisorption on curvature is caused

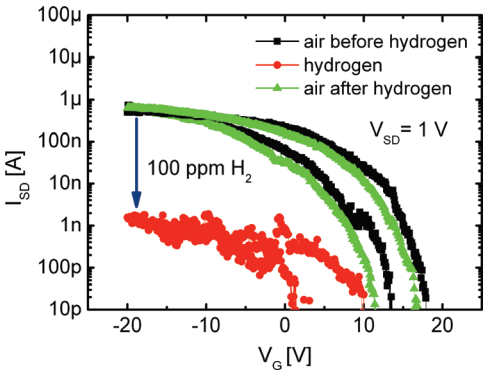

Figure 5. Source−drain current I_{SD} *vs* gate voltage V_G of a 1.4 nm s-SWNT/Pd FET fabricated on parylene-coated Si/SiO_2 substrate. Prior to measurement, the device has been annealed in air at 200 °C for 2 h. The device was then measured under subsequent exposure to air (black squares), 100 ppm H_2 in Ar (red circles), and air again (green triangles). Source−drain voltage is fixed to V_{SD} = 1 V.

by a stronger bond capacity of π orbitals with increasing curvature.[28,30] The binding energy of H to C_{60} is 2.4 eV and hence much larger than the thermal energy.[30]

In our model, we take into account that chemisorption of H can occur on small-diameter SWNTs and thus enhance Φ_{CNT}. The hydrogen sensitivity of s-SWNT/Pd SB-FETs can then be described by

$$G_{ON}/G_{ON}^{H} \propto \exp\{f([\pm\phi_{CNT}(d) - \pm\phi_{Pd} + E_G/2] - [\pm\phi_{CNT}^{H}(d) - \pm\phi_{Pd}^{H} + E_G/2])\}$$

where f is a function for describing either tunneling or thermionic emission.[31] The upper and lower signs are for hole and electron transport, respectively. E_G is the s-SWNT band gap, which is included for completeness but cancels out. The equation shows that no sensitivity is observed if changes of the work functions due to hydrogen exposure are similar for SWNT and Pd: $\phi_{CNT}(d) - \phi_{CNT}^{H}(d) = \phi_{Pd} - \phi_{Pd}^{H}$. Obviously this condition is fulfilled for (6,5)-SWNT/Pd Schottky barriers. The question that arises next is where the atomic hydrogen that chemisorbs on small-diameter SWNTs comes from. In our experiment, the only source of H is the surface of Pd, where H_2 is catalytically dissociated. H has then to diffuse from the Pd surface onto the SWNT in order to bind onto small-diameter SWNTs (inset Figure 3). Such a "spillover" of H has been observed before from metal-oxide catalysts onto multiwalled carbon nanotubes, and we conclude that it occurs also at SWNT−Pd contacts.[32] An interesting experiment would be to expose s-SWNT/Au contacts to atomic hydrogen. The model predicts a large response for small-diameter SWNT devices and no response for large-diameter SWNT devices, assuming an inert and noncatalytic Au surface. So far, we have exposed s-SWNT/Au contacts to molecular hydrogen and observe only a negligible response, as expected (Figure 3 and Figure S7).

Since larger-diameter s-SWNTs were not available to us, we have also studied the hydrogen sensitivity of FLG devices to explore the limit $d \rightarrow \infty$ (Figure 3 and Figure S8). We observe a minute response which we attribute to the absence of Schottky barriers at the FLG/Pd contacts. In line with this conjecture are earlier measurements with $d \sim 3$ nm s-SWNT devices, which yield a comparatively low hydrogen sensitivity of $G_{ON}^{air}/G_{ON}^{H_2} \sim 2$ at a H_2 concentration of 0.5%, that is, 50 times the concentration of our experiments.[15] This weak response is likely due to the small band gap and low Schottky barrier height of larger-diameter s-SWNTs.

The diameter dependence shows that it is important to use sorted carbon nanotubes for sensor fabrication and explains why sensors based on ensembles of unsorted nanotubes have a low sensitivity. So far, 1.4 nm s-SWNT/Pd and (9,7)/Pd FETs show the highest sensitivity with up to 3 orders of magnitude current suppression at 100 ppm H_2. For many sensor applications, the response time is an important parameter. In our 1.4 nm s-SWNT/Pd and (9,7)/Pd FETs, the current changes by a decade within tens of seconds. This is fast compared to previous nanotube-based sensors but still much slower than the experimental time resolution. A diameter dependence of the response time is difficult to extract from the limited number of data points. At present, we observe that the (7,6)-Pd-FET reacts much slower than the 1.4 nm SWNT-FET sensor. In any case, the surface concentration of hydrogen reaches its steady-state value only if the surface is in equilibrium with the bulk and net diffusion into the bulk diminishes.[33] We therefore expect shorter response times for hydrogen adsorption if hydrogen-inert source−drain electrodes covered by a very thin Pd coating are used. We have studied the adsorption and desorption response of hydrogen in Ar and in air. For the adsorption, we see no significant difference; however, we clearly see a promotion of hydrogen desorption by oxygen since switching from H_2/Ar to Ar shows no response in G_{ON} (Figure S9). It was previously reported that adsorbed atomic hydrogen recombines with oxygen (if present) to form water, which desorbs from palladium in a time scale of minutes, hereby considerably enhancing the overall hydrogen desorption rate.[33−35] Our findings (Figure 2 and Supporting Information Figure S9) support this model and are consistent with the results presented in ref 16. The long-term stability is another important parameter for sensor applications. Initially we have seen a substantial reduction of the sensitivity of the s-SWNT/Pd FETs within an hour of measurement. We found out that this aging occurs during measurements and is associated with an overall reduction of I_{SD}. However, the aging occurs likewise in Ar, air, or H_2/Ar. Interestingly, we could completely eliminate this effect by measuring under alternating V_G instead of a constant V_G (Figure 4). All the time-dependent data in this work have been acquired with this alternating V_G protocol. We believe that the aging is due to screening

of the gate field by space charges that propagate from the SWNT into the substrate under constant V_G.[36,37] This causes V_G to become effectively smaller and as a result reduces I_{SD}. Recently, this charge propagation has been imaged on the same time scale by voltage−contrast scanning electron microscopy (VC-SEM), confirming our understanding of the mechanism.[38]The alternating V_G protocol inhibits a buildup of space charge and ensures long-term stability.

In summary, we have shown that the carrier transport through Schottky barrier contacts between Pd and semiconducting single-walled carbon nanotubes is extremely sensitive to hydrogen, with a strong dependence on the nanotube diameter. The detection limit is estimated to 1 ppm for medium-diameter nanotube devices. The large sensitivity for medium-diameter nanotube devices is explained by changes of the Pd work function only. The reduced sensitivity for small-diameter nanotube devices is consistent with an additional change of the nanotube work function due to chemisorption of "spilled-over" atomic hydrogen from the Pd electrode, which compensates the changes in the Pd work function. We have also shown that the long-term stability of the devices depends critically on the biasing protocol of the back gate, due to gate screening by charge accumulation in the substrate. A solution of the problem was presented by a measurement protocol that involves the periodic inversion of the gate voltage. Such devices are interesting hydrogen sensors because they are easy to fabricate, operate in ambient air, work on organic or inorganic substrates, and show superior performance for medium-diameter semiconducting SWNTs.

EXPERIMENTAL SECTION

SB-FETs were produced by combining chirality-selective polymer wrapping (POL) and diameter-selective density-gradient ultracentrifugation (DGU) of SWNTs with dielectrophoretic (DEP) assembling from dispersion. The details of the POL and DGU sorting and of the DEP assembling can be found in refs 39−41. We used four toluene dispersions with s-SWNTs of different chiralities (n,m), as measured by fluorescence spectroscopy (Figure S1). Dispersion POL#1, produced from pulsed laser vaporization material, contains 90% (9,7) SWNT with diameter d = 1.1 nm. Dispersion POL#2, produced from HiPCO material, contains 50% (7,5) and 25% (7,6) SWNT with d = 0.83 and 0.895 nm, respectively. Dispersion POL#3 also produced from HiPCO material contains >90% (7,6) SWNT. Dispersion POL#4, produced from CoMoCat material, contains 75% (6,5) SWNT with d = 0.757 nm. Dispersion DGU#1, produced from arc-discharge material by DGU, contains more than 99% s-SWNTs with a diameter $d = 1.4 \pm 0.2$ nm (Figure S2). Dispersion DGU#2, produced from CoMoCat material by DGU, contains 81% (6,5) tubes with d = 0.757 nm (Figure S3). We also studied few-layer graphene (FLG) devices prepared as in ref 42. Few-layer graphene flakes were obtained by liquid phase exfoliation of graphite in *N*,*N*-dimethylacetamide, using sonication and a subsequent ultracentrifugation step (dispersion FLG#1).[43] The s-SWNTs and FLGs were deposited by dielectrophoresis between Pd(60 nm)/Ti(3 nm) or Au(60 nm)/Ti(3 nm) electrodes on thermally oxidized (200 or 800 nm) p-doped Si(100) substrates (<0.001 Ω·cm). The electrodes were defined by electron beam lithography and metal sputtering (Figure 1a,b). The size of the electrode gaps were adapted to the mean SWNT length and FLG size in the different suspensions, that is, 300 nm for POL#1, POL#2, and POL#4 suspension and 750 nm for DGU#1, DGU#2, POL#3, and FLG#1 suspension. Additional devices were prepared on substrates coated with 100 nm parylene-C, a hydrophobic organic polymer layer, deposited by a chemical vapor deposition technique. We used Raman spectroscopy to confirm the SWNT diameter in our (7,5) devices (Supporting Information Figure S4a) and photoluminescence spectroscopy to confirm the SWNT diameter and chirality in our (9,7) devices on Si/SiO_2 (Supporting Information Figure S4b). A detailed analysis on these devices is provided in ref 44. It was not possible to acquire Raman or photoluminescence data from 1.4 nm s-SWNT devices, due to the restrictions on the excitation wavelengths and detectors in our setups. However, Engel *et al.* provided spectroscopic evidence (Raman, IR-VIS, photo- and electroluminescence) that SWNTs deposited from a dispersion identical to our solution DGU#1 were indeed 99% semiconducting nanotubes with a diameter of $d = 1.4 \pm 0.2$ nm.[45] A detailed analysis of 1.4 nm s-SWNT devices is provided elsewhere.[46] Raman data from a selected FLG device are shown in Supporting Information Figure S4c. The devices were Au or Al wire bonded into a ceramic package for device characterization (Figure 1c). We prepared in total 5× 1.4 nm s-SWNT/Pd, 3× (9,7)/Pd, 1× (7,5)/Pd, 3× (6,5)/Pd, 4× 1.4 nm s-SWNT/Au, 2× (9,7)/Au, 2× (7,6)/Au, 2× (6,5)/Au devices on SiO_2/Si, and 4× 1.4 nm s-SWNT/Pd, 3× (9,7)/Pd, 3× (6,5)/Pd devices on parylene/SiO_2/Si.

The central part of the experimental setup for the measurement of the SB-FETs in controlled atmosphere is a cavity of volume ~1 cm^3 (Figure 1d), which is connected to a gas line system (tube diameter 3 mm) as depicted in Figure 1e. We used copper as the lower half cavity material and pipes from stainless steel tubing to prevent hydrogen poisoning of the system. The ceramic package with the SB-FETs (Figure 1d) forms the upper half of the cavity and is mounted upside down, to close the cavity with an airtight O-ring sealing. The cavity is connected to a four-way valve, which allows the instantaneous switching between gas flow 1 (H_2 in Ar) and gas flow 2 (Ar or air). Another lead joins the pipe system before the cavity for additional optional mixing with gas flow 3 (Ar or air). Gas pressure and flow rate are controlled by pressure gauges and flow meters (dosing valves), respectively. All measurements were carried out at flow rates of Φ = 0.5 L/min, corresponding to a dynamic pressure of $q = 10^{-5}$−10^{-4} bar, and a static gas pressure of p = 1 bar for all three gas flows. For our experiments, the total gas pressure for each flow is given in good approximation by the static gas pressure. The gas in the cavity is exchanged within 0.1 s, which sets the time resolution of our experiment. We use a $1{:}10^4$ mixture of 6 N H_2 and 6 N Ar for gas flow 1, corresponding to 100 ppm H_2, and 6 N Ar or dry air for gas flow 2 and 3. Gas flow 3 allows an optional dilution of gas flow 1 and 2 by adjusting Φ for each gas flow involved. The SB-FETs are electrically connected to Keithley 6430 and Keithley 2400 source measurement units for controlling the source−drain voltage V_{SD}, source−drain current I_{SD}, and the gate voltage V_G, with respect to the grounded drain electrode. A Keithley 7001 switch system allows sequential measurements of different SB-FETs on the same sample chip. All measurements were done at ~300 K.

Acknowledgment. The authors acknowledge D. Resasco and A.C. Ferrari for generous donation of CoMoCat raw material and FLG dispersions, respectively. R.K. acknowledges funding by the Helmholtz-Gemeinschaft Deutscher Forschungszentren (HGF-VH-NG-126), M.C.H. and A.A.G. the National Science

Foundation (DMR-0520513, EEC-0647560, and DMR-0706067) and the Nanoelectronics Research Initiative.

Supporting Information Available: Fluorescence spectra of POL#1−4 (S1); absorption spectra of DGU#1 (S2); fluorescence spectrum of DGU#2 (S3); Raman and fluorescence spectra for (9,7), (7,5) s-SWNT/Pd and FLG/Pd devices on SiO_2 (S4); transport characteristics of (9,7), (7,6), (6,5), and 1.4 nm s-SWNT/Pd devices on SiO_2 (S5); transport characteristics of (9,7), (6,5), and 1.4 nm s-SWNT/Pd devices on SiO_2/parylene (S6); transport characteristics of (9,7), (7,6), (6,5), and 1.4 nm s-SWNT/Au devices on SiO_2 (S7); transport characteristics of FLG devices (S8); response of a 1.4 ± 0.2 nm s-SWNT/Pd FET and a (9,7)-SWNT/Pd device to hydrogen w/o oxygen (S9). This material is available free of charge *via* the Internet at http://pubs.acs.org.

REFERENCES AND NOTES

1. Kinzey, B. R.; Davis, P. B.; Ruiz, A. The Hydrogen Safety Program of the U.S. Department of Energy. In *International Conference on Hydrogen Safety*, Carcassi, M. N., Maragnon, A., Eds.; Elsevier: Amsterdam, The Netherlands, 2005.
2. National Hydrogen Energy Roadmap, United States Department of Energy, 2002
3. Korotcenkov, G.; Han, S. D.; Stetter, J. R. Review of Electrochemical Hydrogen Sensing. *Chem. Rev.* **2009,** *109*, 1402–1433.
4. Niemann, H. B.; Atreya, S. K.; Carignan, G. R.; Donahue, T. M.; Haberman, J A.; Harpold, D N.; Hartle, R E.; Hunten, D. M.; Kasprzak, W T.; Mahaffy, P. R.; *et al.* The Galileo Probe Mass Spectrometer: Composition of Jupiter's Atmosphere. *Science* **1996,** *272*, 846–849.
5. Yang, F.; Taggart, D.; Penner, R. M. Fast, Sensitive Hydrogen Gas Detection Using Single Palladium Nanowires That Resist Fracture. *Nano Lett.* **2009,** *9*, 2177–2182.
6. Tardy, P.; Coulon, J.-R.; Lucat, C.; Mesnil, F. Dynamic Thermal Conductivity Sensor for Gas Detection. *Sens. Actuators, B* **2004,** *98*, 63–68.
7. Drake, C.; Deshpande, S.; Bera, D.; Seal, S. Metallic Nanostructured Materials Based Sensors. *Int. Mater. Rev.* **2007,** *52*, 289–317.
8. Lundström, I.; Shivaraman, M. S.; Svensson, M. S. A Hydrogen Sensitive Pd-Gate MOS Transistor. *J. Appl. Phys.* **1975,** *46*, 3876–3881.
9. Favier, F.; Walter, E.; Zach, M.; Bentner, Th.; Penner, R. M. Hydrogen Sensors and Switches from Electrodeposited Palladium Mesowire Arrays. *Science* **2001,** *293*, 2227–2231.
10. Baik, J. M.; Kim, M. H.; Larson, C; Yavuz, C. T.; Stucky, G.; Wodtke, A. M.; Moskovits, M. Pd-Sensitized Single Vanadium-Oxide Nanowire: Highly Responsive Hydrogen Sensing Based on the Mott Transition. *Nano Lett.* **2009,** *9*, 3980–3984.
11. Conrad, H.; Ertl, G.; Latta, E. Adsorption of Hydrogen on Palladium Single Crystal Surfaces. *Surf. Sci.* **1974,** *41*, 435–446.
12. Dus, R.; Nowakowski, R.; Nowicka, E. Chemical and Structural Components of Work Function Changes in the Process of Palladium Hydride Formation within Thin Pd Films. *J. Alloys Compd.* **2005,** *404−406*, 284–287.
13. Svensson, J.; Sourab, A. A.; Tarakanov, Y.; Lee, D. S.; Park, S. J.; Baek, S. J.; Park, Y. W.; Campbell, E. The Dependence of the Schottky Barrier Height on Carbon Nanotube Diameter for Pd-Carbon Nanotube Contacts. *Nanotechnology* **2009,** *20*, 175204-1–175204-5.
14. Heinze, S.; Tersoff, J.; Martel, R.; Derycke, V.; Appenzeller, J.; Avouris, Ph. Carbon Nanotubes as Schottky Barrier Transistors. *Phys. Rev. Lett.* **2002,** *89*, 106801-1–106801-4.
15. Javey, A.; Guo, J.; Wang, Q.; Lundstrom, M.; Dai, H. Ballistic Carbon Nanotube Field Effect Transistors. *Nature* **2003,** *424*, 654–657.
16. Hayakawa, Y.; Suda, Y.; Hashizume, T.; Sugawara, H.; Sakai, Y. Hydrogen-Sensing Response of Carbon-Nanotube Thin-Film Sensor with Pd Comb-like Electrodes. *Jpn. J. Appl. Phys.* **2007,** *46*, L362–L364.
17. Wong, Y. M.; Kang, W. P.; Davidson, J. L.; Wisitsora, A.; Soh, K. L. A Novel Microelectronic Gas Sensor Utilizing Carbon Nanotubes for Hydrogen Gas Detection. *Sens. Actuators, B* **2003,** *93*, 327–332.
18. Suehiro, J.; Hidaka, S.; Yamane, S.; Imasaka, K. Fabrication of Interfaces between Carbon Nanotubes and Catalytic Palladium Using Dielectrophoresis and Its Application to Hydrogen Gas Sensor. *Sens. Actuators, B* **2007,** *127*, 505–511.
19. Khalap, V. R; Sheps, T.; Kane, A. A.; Collins, P. G. Hydrogen Sensing and Sensitivity of Palladium Decorated Single-Walled Carbon Nanotubes with Defects. *Nano Lett.* **2010,** *10*, 896–901.
20. Sippel-Oakley, J.; Wang, H.-T.; Kang, B. S.; Wu, Z.; Ren, F.; Rinzler, A. G.; Pearton, S. J. Carbon Nanotube Films for Room Temperature Hydrogen Sensing. *Nanotechnology* **2005,** *16*, 2218–2221.
21. Sun, X.; Sun, Y. Single-Walled Carbon Nanotubes for Flexible Electronics and Sensors. *J. Mater. Sci. Technol.* **2008,** *24*, 569–577.
22. Kong, J.; Chapline, M. G.; Dai, H. Functionalized Carbon Nanotubes for Molecular Hydrogen Sensors. *Adv. Mater.* **2001,** *13*, 1384–1386.
23. Ding, D.; Chen, Z.; Rajaputra, S.; Singh, V. Hydrogen Sensors Based on Aligned Carbon Nanotubes in an Anodic Aluminum Oxide Template with Palladium as a Top Electrode. *Sens. Actuators, B* **2007,** *124*, 12–17.
24. Krishnakumar, M.; Ramaprabhu, S. Palladium Dispersed Multiwalled Carbon Nanotube Based Hydrogen Sensor for Fuel Cell Application. *Int. J. Hydrogen Energy* **2007,** *32*, 2518–2526.
25. Mubeen, S.; Zhang, T.; Yoo, B.; Deshusses, M.a.; Myung, N. V. Palladium Nanoparticles Decorated Single-Walled Carbon Nanotube Hydrogen Sensor. *J. Phys. Chem. C* **2007,** *111*, 6321–6327.
26. Sayago, I.; Terrado, E.; Lafuente, E.; Horrillo, M.; Maser, W.; Benito, A.; Navarro, R.; Urriolabeitia, E.; Martinez, M.; Gutierrez, J. Hydrogen Sensors Based on Carbon Nanotubes Thin Films. *Sens. Actuators, B* **2007,** *122*, 15–19.
27. Alonso, J.; Arellano, J. S.; Molina, L. M.; Rubio, A.; Lopez, M. J. Interaction of Molecular and Atomic Hydrogen with Single-Wall Carbon Nanotubes. *IEEE Trans. Nanotechnol.* **2004,** *3*, 304–310.
28. Ruffieux, P.; Gröning, O.; Bielmann, M.; Mauron, P.; Schlapbach, L.; Gröning, P. Hydrogen Adsorption on sp^2-Bonded Carbon: Influence of the Local Curvature. *Phys. Rev. B* **2002,** *66*, 245416-1–245416-6.
29. Zecho, T.; Güttler, A.; Sha, X.; Jackson, B.; Küppers, J. Adsorption of Hydrogen and Deuterium Atoms on the (0001) Graphite Surface. *J. Phys. Chem.* **2002,** *117*, 8486–8492.
30. Park, S.; Srivastava, D.; Cho, K. Local Reactivity of Fullerenes and Nanodevice Applications. *Nanotechnology* **2001,** *12*, 245–249.
31. Appenzeller, J.; Radosavljević, M.; Knoch, J.; Avouris, Ph. Tunneling *versus* Thermionic Emission in One-Dimensional Semiconductors. *Phys. Rev. Lett.* **2004,** *92*, 048301-1–048301-5.
32. Lueking, A.; Yang, R. T. Hydrogen Spillover from a Metal-Oxide Catalyst onto Carbon Nanotubes—Implications for Hydrogen Storage. *J. Catal.* **2002,** *206*, 165–168.
33. Lundström, I.; Söderberg, D. Hydrogen Sensitive MOS Structures Part 2: Characterization. *Sens. Actuators* **1981,** *2*, 105–138.
34. Petersson, L.; Dannetun, H.; Lundström, I. The Water-Forming Reaction on Palladium. *Surf. Sci.* **1985,** *161*, 77–100.
35. Salomonsson, A.; Eriksson, M.; Dannetun, H. Hydrogen Interaction with Platinum and Palladium Metal−Insulator−Semiconductor Devices. *J. Appl. Phys.* **2005,** *98*, 014505-1–014505-10.
36. Vijayaraghavan, A.; Kar, S.; Soldano, C.; Talapatra, S.; Nalamasu, O.; Ajayan, P. M. Charge-Injection Induced Dynamic Screening and Origin of Hysteresis in Field-Modulated Transport in Single-Wall Carbon Nanotubes. *Appl. Phys. Lett.* **2006,** *89*, 162108-1–162108-3.

37. Kar, S.; Vijayaraghavan, A.; Soldano, C.; Talapatra, S.; Vajtai, R.; Nalamasu, O.; Ajayan, P. M. Quantitative Analysis of Hysteresis in Carbon Nanotube Field Effect Devices. *Appl. Phys. Lett.* **2006,** *89*, 132118-1–132118-3.
38. Vijayaraghavan, A.; Marquardt, C. W.; Dehm, S.; Hennrich, F.; Krupke, R. Imaging Defects and Junctions in Single-Walled Carbon Nanotubes by Voltage-Contrast Scanning Electron Microscopy. *Carbon* **2010,** *48*, 494–502.
39. Hennrich, F.; Lebedkin, S.; Kappes, M. M. Improving Separation Techniques for Single-Walled Carbon Nanotubes: Towards Monodisperse Samples. *Phys. Status Solidi B* **2008,** *245*, 1951–1953.
40. Vijayaraghavan, A.; Blatt, S.; Weissenberger, D.; Oron-Carl, M.; Hennrich, F.; Gerthsen, D.; Hahn, H.; Krupke, R. Ultra Large Scale Directed Assembly of Single Walled Carbon Nanotube Devices. *Nano Lett.* **2007,** *7*, 1556–1560.
41. Arnold, M. S.; Green, A. A.; Hulvat, J. F.; Stupp, S. I.; Hersam, M. C. Sorting Carbon Nanotubes by Electronic Structure Using Density Differentiation. *Nat. Nanotechnol.* **2006,** *1*, 60–65.
42. Vijayaraghavan, A.; Sciascia, C.; Dehm, S.; Lombardo, A.; Bonetti, A.; Ferrari, A. C.; Krupke, R. Dielectrophoretic Assembly of High-Density Arrays of Individual Graphene Devices for Rapid Screening. *ACS Nano* **2009,** *3*, 1729–1734.
43. Hernandez, Y.; Nicolosi, V.; Lotya, M.; Blighe, F. M.; Sun, Z.; De, S.; McGovern, I. T.; Holland, B.; Byrne, M.; Gun'Ko, Y. K.; *et al.* High Yield Production of Graphene by Liquid Phase Exfoliation of Graphite. *Nat. Nanotechnol.* **2008,** *3*, 563–566.
44. Vijayaraghavan, A.; Hennrich, F.; Stürzl, N.; Engel, M.; Ganzhorn, M.; Oron-Carl, M.; Marquardt, C.; Dehm, S.; Lebedkin, S.; Kappes, M. M.; *et al.* Towards Single-Chirality Carbon Nanotube Devices. *ACS Nano* **2010,** *4*, 2748–2754.
45. Engel, M.; Small, J. P.; Steiner, M.; Freitag, M.; Green, A.; Hersam, M. C.; Avouris, Ph. Thin Film Nanotube Transistors Based on Self-Assembled, Aligned, Semiconducting Carbon Nanotube Arrays. *ACS Nano* **2009,** *3*, 2445–2452.
46. Ganzhorn, M.; Vijayaraghavan, A.; Green, A. A.; Dehm, S.; Voigt, A.; Rapp, M.; Hersam, M. C.; Krupke, R. Scalable, CMOS-Compatible Assembly of Ambipolar Semiconducting Single-Wall Carbon Nanotube Devices. *Adv. Mater.* **2011**, DOI: 10.1002/adma.201004640.
47. Hamada, N.; Sawada, S.; Oshiyama, A. New One Dimensional Conductors: Graphitic Microtubules. *Phys. Rev. Lett.* **1992,** *47*, 1579–1581.